ISSN 0021-3640, JETP Letters, 2019, Vol. 110, No. 9, pp. 624–628. © Pleiades Publishing, Inc., 2019.
Russian Text © The Author(s), 2019, published in Pis'ma v Zhurnal Eksperimental'noi i Teoreticheskoi Fiziki, 2019, Vol. 110, No. 9, pp. 622–627.

CONDENSED MATTER

Phase Transformations in Copper–Tin Solid Solutions at High-Pressure Torsion

B. B. Straumal[a, b, c, d, *], A. R. Kilmametov[c, d], I. A. Mazilkin[a, c, d], A. Korneva[e], P. Zieba[e], and B. Baretzky[d]

[a] *Institute of Solid State Physics, Russian Academy of Sciences, Chernogolovka, Moscow region, 142432 Russia*
[b] *Chernogolovka Research Center, Russian Academy of Sciences, Chernogolovka, Moscow region, 142432 Russia*
[c] *National University of Science and Technology MISiS, Moscow, 119049 Russia*
[d] *Institute of Nanotechnology, Karlsruhe Institute of Technology, 76344 Eggenstein-Leopoldshafen, Germany*
[e] *Institute of Metallurgy and Materials Science, Polish Academy of Sciences, 30-059 Kraków, Poland*
**e-mail: straumal@issp.ac.ru*

Received September 13, 2019; revised October 6, 2019; accepted October 6, 2019

Phase transformations of some Hume–Rothery phases (electron compounds) to others in a copper–tin system subjected to high-pressure torsion were detected in our previous work [B.B. Straumal et al., JETP Lett. **100**, 376 (2014)]. In particular, the torsion of the $\zeta + \varepsilon$ phase mixture at high pressure led to the formation of the $\delta + \varepsilon$ phase mixture, as after long-term annealing in the temperature interval $T_{\text{eff}} = 350–589$°C. In this work, it has been shown that the high-pressure torsion of α-solid solutions of tin in copper results in the final stable solid solution whose composition is independent of the composition of the initial α phase before high-pressure torsion. The final composition is the same as after long-term annealing at the temperature $T_{\text{eff}} = (420 \pm 10)$°C. The rate of high-pressure torsion-induced mass transfer is several orders of magnitude higher than the rate of conventional thermal diffusion at the treatment temperature T_{HPT} and is close to values at T_{eff}. This occurs because high-pressure torsion increases the concentration of lattice defects and this increase is in turn equivalent to an increase in the temperature.

DOI: 10.1134/S0021364019210112

Severe plastic deformation can induce phase transitions in condensed matter [1–7]. This means that phases in a sample after severe plastic deformation will be different from those before severe plastic deformation. In particular, crystalline phases can be transformed to amorphous phases [8–12] and vice versa [11, 13, 14]. The decomposition of a supersaturated solid solution can compete at severe plastic deformation with the solution of particles of the second phase in the matrix [2, 15–17]. Severe plastic deformation can induce transformations between different possible allotropic modifications of a metal (e.g., α–ε Co, α–γ Fe, α–β–ω Ti, α–β–ω Zr or hBN–wBN) [18–25]. Phase transformations with mass transfer can be combined with martensitic transformations [26, 27]. In more complex cases, one can observe transformations between intermetallics, e.g., between Hume–Rothery phases (electron compounds) [16, 28]. Hume–Rothery phases appear when the matrix formed by univalent atoms (such as gold, copper, or silver) is supplemented by atoms with a higher valence (zinc, tin, indium, etc.) [29, 30]. In particular, the equilibrium composition of the Cu–24 at % Sn alloy varies with increasing temperature from $\alpha + \varepsilon$ (at $T < 350$°C) through $\delta + \varepsilon$ (at 350°C $< T <$ 589°C) and $\zeta + \varepsilon$ (at 589°C $< T <$ 640°C) to γ (at 640°C $< T <$ 700°C) [28]. Severe plastic deformation by high-pressure torsion of the initial sample with the $\zeta + \varepsilon$ phase mixture results in the formation of the $\delta + \varepsilon$ phase mixture. In other words, the phases appearing in the alloy after high-pressure torsion are the same as if it were annealed in the temperature range of $T_{\text{eff}} = 350–589$°C. The phases formed in the sample at severe plastic deformation in other experiments also exist on equilibrium phase diagrams at a certain effective temperature T_{eff}. In other words, these phases are those as if the sample were annealed at an increased temperature T_{eff} for a long time. Meanwhile, the process of severe plastic deformation occurs at room temperature for a short time (usually several minutes). The aim of this work is to study the high-pressure torsion of the Cu–8.1 at % Sn alloy with a lower tin content than in [28]. We expected that the high-pressure torsion of the alloy would lead not to the mutual transformation of intermetallics as in [28] but to the formation $\leftrightarrow$ decomposition reaction of the solid solution similar to those we observed in other copper alloys [2, 15, 17]. Our aim is

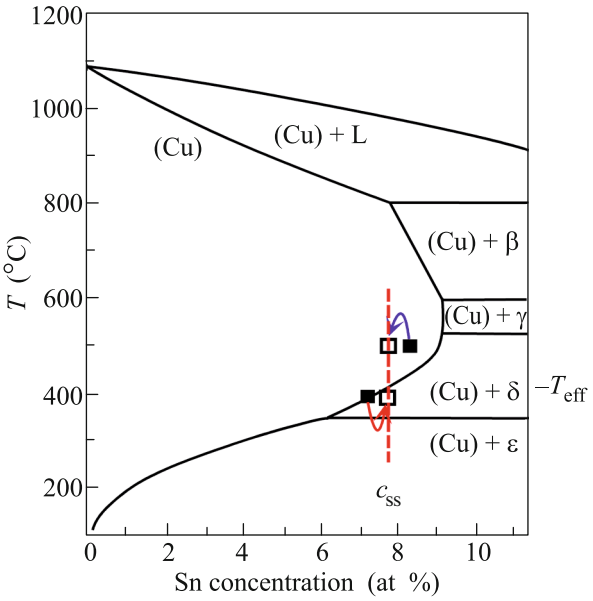

Fig. 1. (Color online) Part of the phase diagram of Cu–Sn [31]. Thick solid lines indicate first-order phase transitions. Closed squares mark the compositions of the solid solution annealed at 400 and 500°C before high-pressure torsion. Open squares indicate the compositions of the solid solution after high-pressure torsion. The vertical dashed straight line shows the equifinal concentration c_{ss} in the solid solution after high-pressure torsion.

to determine whether the effective temperature in this case correlates with the value $T_{eff} = 350–589$°C differs from that for the transformations of intermetallics in [28].

For our experiments, we prepared Cu–8.1 at % Sn alloy ingots 10 mm in diameter by means of vacuum induction melting of copper and tin with a purity of 99.998 wt %. These ingots were cut into 0.7-mm-thick disks by means of spark cutting. These disks were sealed in evacuated quartz ampules with a residual pressure of 4×10^{-4} Pa. The ampules with the samples were annealed in a SUOL electric resistance furnace at a temperature of 400°C for 888 h and at a temperature of 500°C for 894 h. Points corresponding to annealing temperatures and concentrations of the alloy with 8.1 wt % tin lie on the phase diagram of Cu–Sn (Fig. 1 [31]) in the regions (Cu) + δ and (Cu), respectively. After annealing, the samples were quenched in water (the ampoules were broken). After annealing and quenching, the samples were subjected to high-pressure torsion in a Bridgman anvil cell (W. Klement GmbH, Lang, Austria) at room temperature and a pressure of 7 GPa for five turns of anvils at a rate of 1 rpm. In this regime, a steady state is reached in the sample already after one and a half turns of anvils; in this state, the torsional moment of the device for high-pressure torsion is saturated and does not change at further deformation [2, 15, 17]. The steady state is also reached at the high-pressure torsion of other materials [32–34]. The samples for structural studies were mechanically ground and polished using a diamond paste with a grain size down to 1 μm. The samples after high-pressure torsion were cut at a distance of 3 mm from the center of a deformed disk. The prepared slices were examined by means of scanning electron microscopy and X-ray microanalysis with a Philips XL30 scanning electron microscope equipped with a LINK ISIS (Oxford Instruments) energy-dispersive X-ray spectrometer. X-ray diffraction patterns were obtained in the Bragg–Brentano geometry on a Philips X'Pert powder diffractometer with Cu $K\alpha$ radiation. The lattice constant was determined using Fityk software [35]. Phases in the alloys were identified by comparing with the X'Pert HighScore Panalytical phase databank. The transmission electron microscopy analysis was performed with a TECNAI G2 FEG super TWIN (200 kV) microscope equipped with an EDAX energy-dispersive spectrometer. Thin-film samples for the transmission electron microscopy analysis were prepared by the electropolishing method with an Electrolyte D2 (Struers) device.

Figure 2 shows (a) the scanning electron microscopy image of the Cu–8.1 at % Sn alloy annealed at a temperature of 400°C for 888 h, (b) bright and (c) dark-field transmission electron microscopy images of the same alloy annealed at 500°C for 894 h after high-pressure torsion, and (d) selected area diffraction pattern. The electron microscopy studies and X-ray diffraction patterns show that the samples annealed at 500°C for 894 h contained only a Cu-based α-solid solution with an fcc lattice and a lattice constant of 0.3692 nm. The composition of the samples annealed at 500°C for 894 h is marked by the closed square at 500°C on the phase diagram in Fig. 1. Figure 3 shows the dependence of the lattice constant of the fcc solid solution of tin in copper on the tin content plotted using the data from [35–40]. The lattice constant increases linearly from 0.3621 nm in the solid solution with 0.6 at % Sn to 0.3702 nm in the solid solution with 8.5 at % Sn. Such a linear dependence is known as Vegard's law valid for ideal solid solutions [41]. The lattice constant in the sample annealed at 500°C for 894 h is also marked by the closed black square in Fig. 3. The samples annealed at 400°C for 888 h contained two phases: δ intermetallic and Cu-based α-solid solution with the fcc lattice and a lattice constant of 0.36872 nm. The δ (or $Cu_{41}Sn_{11}$) phase has a cubic structure with the space group F-43m and the lattice constant $a = 1.79632$ nm. The lattice constant 0.36872 nm of the sample annealed at 400°C for 888 h is also marked by the closed black square in Fig. 3. The lattice constant 0.36872 nm corresponds to a content of 7.1 at %, which is below 8.1 at % because some amount of tin is contained in δ intermetallic crystals. The corresponding closed square on the phase diagram in Fig. 1 is located at 400°C on the solvus of tin in copper. Figure 2a shows one of the

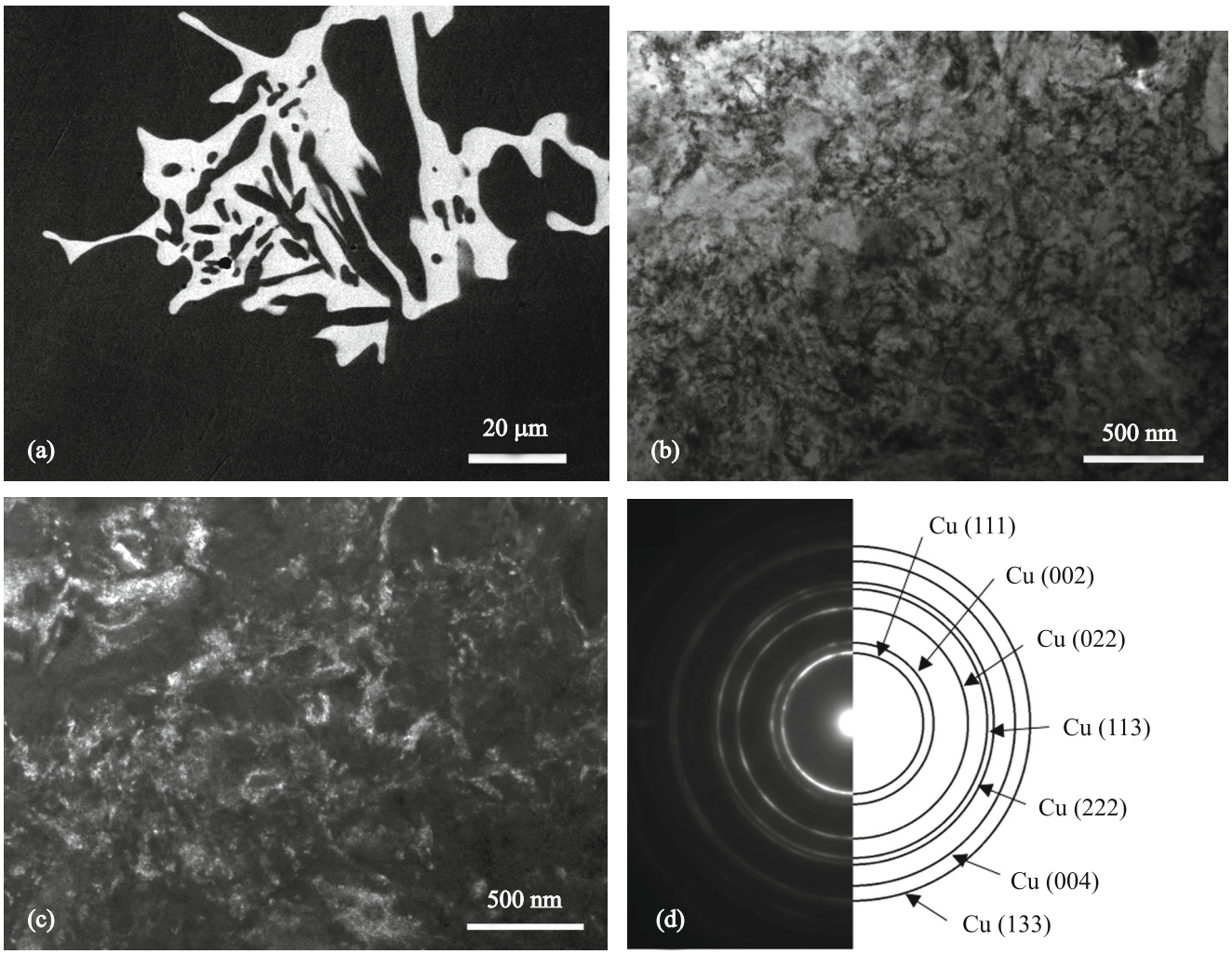

Fig. 2. (a) Scanning electron microscopy image of the Cu–8.1 wt % Sn alloy annealed at 400°C for 888 h. (b) Bright and (c) dark-field scanning electron microscopy images and (d) the selected area diffraction pattern of the same alloy annealed at 500°C for 894 h after high-pressure torsion.

δ-phase crystals (light) surrounded by the matrix of the Cu-based α-solid solution (dark).

The size of grains in the sample after high-pressure torsion decreases sharply from tens and hundreds of microns in annealed samples to about 150 nm (see the microstructures shown in Figs. 2b and 2c). Peaks on X-ray diffraction spectra are significantly broadened and points on electron diffraction rings are joined in almost solid lines (see Fig. 2d). A grain size of 150 nm is typical of copper alloys after high-pressure torsion [2]. The lattice constant in the solid solution of the sample annealed at 500°C for 894 h decreases from 0.36962 nm (the closed square on the straight line of Vegard's law in Fig. 3 and on the phase diagram in Fig. 1) to 0.36935 nm (the open square on the straight line of Vegard's law in Fig. 3 and on the phase diagram in Fig. 1). This indicates a decrease in the tin content in the solid solution (Cu) and its partial decomposition. The lattice constant in the solid solution of the sample annealed at 400°C for 888 h increases from 0.36872 nm (the closed square on the straight line of Vegard's law in Fig. 3 and on the phase diagram in Fig. 1) to 0.36925 nm (the open square on the straight line of Vegard's law in Fig. 3 and on the phase diagram in Fig. 1). This indicates an increase in the tin content in the solid solution (Cu) and a partial solution of the second δ phase.

It is remarkable that the lattice constants in the (Cu) solid solution after high-pressure torsion in both samples are almost the same (0.36935 and 0.36925 nm). This means that there is a certain concentration c_{ss} established at high-pressure torsion in the steady state for the solid solution of tin in copper. If the initial concentration c_{init} in the solid solution is below c_{ss}, it increases at high-pressure torsion. If the initial concentration c_{init} in the solid solution is above c_{ss}, it decreases at high-pressure torsion to c_{ss}. Such a property is called equifinality of the steady state (this notion was introduced by von Bertalanffy [42]). It

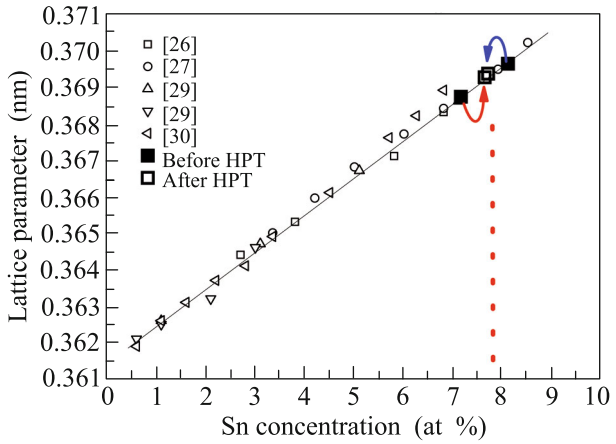

Fig. 3. (Color online) Lattice constant of Cu–Sn solid solutions versus the tin content (Vegard's law). Small symbols are data taken from [36–40]. Large symbols are the lattice constants in the samples annealed at 400 and 500°C before and after high-pressure torsion obtained in this work.

serves as a certain attractor; i.e., other states approach it at high-pressure torsion, as, e.g., observed at the decomposition ↔ formation of the solid solution in copper–silver [15] and copper–cobalt [17] alloys.

It is seen in the phase diagram in Fig. 1 that the red vertical dashed line at the concentration c_{ss} intersects the solvus of tin in copper at a temperature of (420 ± 10)°C. This means that the concentration in the (Cu) solid solution after high-pressure torsion is such as if the samples were annealed for a long time at the temperature T_{eff} = (420 ± 10)°C. This temperature is called the effective temperature and lies in the effective temperature range T_{eff} = 350–589°C, which we previously determined from the $\zeta + \varepsilon \rightarrow \delta + \varepsilon$ transformation. Agreement between temperatures T_{eff} for transformations between Hume–Rothery phases and formation ↔ decomposition transformations of the (Cu) solid solution means that the transformation mechanism is the same in both cases. We believe that this mechanism is the dynamic growth/solution of grains of the solid solution and/or intermetallic owing to the transition of tin atoms from one phase to another through the interface [15].

Thus, high-pressure torsion stimulates mass transfer similar to diffusion. We now compare deformation-induced mass transfer to conventional thermal diffusion. To this end, we formally estimate the bulk diffusion coefficient D_{HPT} necessary for such a mass transfer by the formula $L = (D_{HPT}t)^{0.5}$. The duration t of high-pressure torsion is 300 s. The distance L to which the mass is transferred can be estimated as a half of the grain size after high-pressure torsion, i.e., $L \sim 70$ nm. Correspondingly, $D_{HPT} \sim 10^{-16}$ m^2/s. The extrapolation of D for bulk self-diffusion in copper to 300 K (temperature of high-pressure torsion T_{HPT}) and bulk diffusion of tin in copper gives the values $D = 10^{-35}$ m^2/s [43] and $D = 10^{-31}$ m^2/s [44], respectively. Although compression reduces the bulk and grain-boundary diffusion coefficients [45, 46], the D_{HPT} value is 13–17 orders of magnitude higher than these extrapolated values. This means that high-pressure torsion strongly accelerates mass transfer, as in our preceding experiments.

The extrapolation of the diffusion coefficient to T_{eff} rather than to the temperature of high-pressure torsion T_{HPT} = 300 K gives $D = 10^{-17}$ m^2/s [43] and $D = 10^{-15}$ m^2/s [44] for the bulk self-diffusion of copper and bulk diffusion of tin in copper, respectively. These values almost coincide with D_{HPT}. This phenomenon can be explained by an increased concentration of defects (in particular, vacancies) in the steady state at high-pressure torsion, which is equivalent to an increase in the temperature.

To summarize, we have revealed that high-pressure torsion in the copper–tin system results not only in phase transformations of some Hume–Rothery phases (electron compounds) to others but also in competition between the decomposition and formation of the solid solution of tin in copper. In this case, a certain stationary concentration c_{ss} is established, which is independent of the initial conditions (the concentration in the initial solid solution c_{init} before high-pressure torsion), i.e., is equifinal. The concentration c_{ss} is such as if the samples were annealed for a long time at the temperature T_{eff} = (420 ± 10)°C. This temperature is called the effective temperature and lies in the effective temperature range T_{eff} = 350–589°C, which we previously determined from the $\zeta + \varepsilon \rightarrow \delta + \varepsilon$ transformation. The observed decomposition/formation of the (Cu) solid solution requires mass transfer. Its rate is 13–17 orders of magnitude higher than the rate of conventional thermal diffusion at room temperature (i.e., at the temperature of high-pressure torsion T_{HPT}). However, the rate of mass transfer is close to the rate of diffusion at T_{eff}. This phenomenon is apparently explained by an increased concentration of defects (in particular, vacancies) in the steady state at high-pressure torsion, which is in turn equivalent to an increase in the temperature from T_{HPT} to T_{eff}.

Strictly speaking, high-pressure torsion is not equivalent to an increase in the temperature and even is not equivalent to the acceleration of diffusion [5–7, 23–27]. At high-pressure torsion, mass transfer occurs at large distances from nanometers to millimeters. In this process, a huge number of different defects are produced (and disappear). In particular, high-pressure torsion is often accompanied by the amorphization of alloys, which is not observed at their heating [11, 12]. As a result, the final picture is close to that observed at an increase in the temperature [47–49].

FUNDING

This work was performed in part within the state assignment for the Institute of Solid State Physics, Russian Academy of Sciences, and the Chernogolovka Research Center, Russian Academy of Sciences, and was supported by the Russian Foundation for Basic Research (project no. 18-33-00473) and Narodowe Centrum Nauki of Poland (project no. OPUS 2014/13/B/ST8/04247).

REFERENCES

1. X. Sauvage, A. Chbihi, and X. Quelennec, J. Phys. Conf. Ser. **240**, 012003 (2010).
2. B. B. Straumal, A. R. Kilmametov, A. Korneva, A. A. Mazilkin, P. B. Straumal, P. Zieba, and B. Baretzky, J. Alloys Compd. **707**, 20 (2017).
3. S. K. Pabi, J. Joardar, and B. S. Murty, Proc. Indian Natl. Sci. Acad. A **67**, 1 (2001).
4. B. B. Straumal, A. R. Kilmametov, Yu. Ivanisenko, A. A. Mazilkin, O. A. Kogtenkova, L. Kurmanaeva, A. Korneva, P. Zieba, and B. Baretzky, Int. J. Mater. Res. **106**, 657 (2015).
5. V. I. Levitas and O. M. Zarechnyy, Phys. Rev. B **82**, 174123 (2010).
6. M. Javanbakht and V. I. Levitas, Phys. Rev. B **94**, 214104 (2016).
7. V. I. Levitas, Mater. Trans. **60**, 1294 (2019).
8. S. D. Prokoshkin, I. Yu. Khmelevskaya, S. V. Dobatkin, I. B. Trubitsyna, E. V. Tatyanin, V. V. Stolyarov, and E. A. Prokofiev, Acta Mater. **53**, 2703 (2005).
9. X. Sauvage, L. Renaud, B. Deconihout, D. Blavette, D. H. Ping, and K. Hono, Acta Mater. **49**, 389 (2001).
10. A. A. Mazilkin, G. E. Abrosimova, S. G. Protasova, B. B. Straumal, G. Schütz, S. V. Dobatkin, and A. S. Bakai, J. Mater. Sci. **46**, 4336 (2011).
11. V. I. Levitas, Phys. Rev. Lett. **95**, 075701 (2005).
12. V. I. Levitas, Y. Ma, E. Selvi, J. Wu, and J. A. Patten, Phys. Rev. B **85**, 054114 (2012).
13. A. M. Glezer, M. R. Plotnikova, A. V. Shalimova, and S. V. Dobatkin, Bull. Russ. Acad. Sci.: Phys. **73**, 1233 (2009).
14. S. Hóbor, Á. Révész, A. P. Zhilyaev, and Zs. Kovacs, Rev. Adv. Mater. Sci. **18**, 590 (2008).
15. B. B. Straumal, B. Baretzky, A. A. Mazilkin, F. Phillipp, O. A. Kogtenkova, M. N. Volkov, and R. Z. Valiev, Acta Mater. **52**, 4469 (2004).
16. B. B. Straumal, S. G. Protasova, A. A. Mazilkin, E. Rabkin, D. Goll, G. Schütz, B. Baretzky, and R. Valiev, J. Mater. Sci. **47**, 360 (2012).
17. B. B. Straumal, A. R. Kilmametov, Yu. O. Kucheev, L. Kurmanaeva, Yu. Ivanisenko, B. Baretzky, A. Korneva, P. Zieba, and D. A. Molodov, Mater. Lett. **118**, 111 (2014).
18. B. B. Straumal, A. A. Mazilkin, B. Baretzky, E. Rabkin, and R. Z. Valiev, Mater. Trans. **53**, 63 (2012).
19. Y. Ivanisenko, I. MacLaren, X. Sauvage, R. Z. Valiev, and H.-J. Fecht, Acta Mater. **54**, 1659 (2006).
20. M. T. Pérez-Prado and A. P. Zhilyaev, Phys. Rev. Lett. **102**, 175504 (2009).
21. K. Edalati, E. Matsubara, and Z. Horita, Metall. Mater. Trans. A **40**, 2079 (2009).
22. Y. Ivanisenko, A. Kilmametov, H. Roesner, and R. Valiev, Int. J. Mater. Res. **99**, 36 (2008).
23. B. Feng and V. I. Levitas, Mater. Sci. Eng. A **680**, 130 (2017).
24. B. Feng, V. I. Levitas, and M. Kamrani, Mater. Sci. Eng. A **731**, 623 (2018).
25. B. Feng, V. I. Levitas, and W. Li, Int. J. Plast. **113**, 236 (2019).
26. B. B. Straumal, A. R. Kilmametov, G. A. Lopez, I. López-Ferreño, M. L. No, J. San Juan, H. Hahn, and B. Baretzky, Acta Mater. **125**, 274 (2017).
27. T. Kim, G. Ouyang, J. D. Poplawsky, M. J. Kramer, V. I. Levitas, J. Cui, and L. Zhou, J. Alloys Compd. **808**, 151743 (2019).
28. B. B. Straumal, A. R. Kilmametov, Yu. O. Kucheev, K. I. Kolesnikova, A. Korneva, P. Zieba, and B. Baretzky, JETP Lett. **100**, 376 (2014).
29. V. F. Degtyareva and Yu. A. Skakov, Sov. Phys. Crystallogr. **21**, 222 (1976).
30. Ya. S. Umanskii and Yu. A. Skakov, *Physics of Metals: Atomic Structure of Metals and Alloys* (Metallurgiya, Moscow, 1978) [in Russian].
31. S. Fürtauer, D. Li, D. Cupid, and H. Flandorfer, Intermetallics **34**, 142 (2013).
32. K. Bryla, J. Morgiel, M. Faryna, K. Edalati, and Z. Horita, Mater. Lett. **212**, 323 (2018).
33. K. Edalati, D. J. Lee, T. Nagaoka, M. Arita, H. S. Kim, Z. Horita, and R. Pippan, Mater. Trans. **57**, 533 (2016).
34. K. Edalati, Z. Horita, T. Furuta, and S. Kuramoto, Mater. Sci. Eng. A **559**, 506 (2013).
35. M. Wojdyr, J. Appl. Crystallogr. **43**, 1126 (2010).
36. E. A. Owen and J. Iball, J. Inst. Met. **57**, 267 (1935).
37. C. Haase and F. Pawlek, Z. Metallkd. **28**, 73 (1936).
38. S. T. Konobeevskii and W. P. Tarrassova, Acta Physicochim. U.R.S.S. **6**, 781 (1937).
39. A. P. Gulyaev and E. E Trusova, Zh. Tekh. Fiz. **20**, 66 (1950).
40. A. F. Anderson, Trans. Met. Soc. AIME **212**, 259 (1958).
41. L. Vegard, Z. Phys. **5**, 17 (1921).
42. L. von Bertalanffy, Science (Washington, DC, U. S.) **111**, 23 (1950).
43. S. Fujikawa and K. I. Hirano, in *Proceedings of 5th Yamada Conference on Point Defects, Defect Interactions in Metals,* Ed. by J. I. Takamura, M. Doyama, and M. Kiritani (Univ. Tokyo Press, Tokyo, 1982), p. 554.
44. V. A. Gorbachev, S. M. Klotsman, Ya. A. Rabovskiy, V. K. Talinskiy, and A. N. Timofeyev, Sov. Phys. Met. Metallogr. **35**, 226 (1973).
45. B. B. Straumal, L. M. Klinger, and L. S. Shvindlerman, Scr. Met. **17**, 275 (1983).
46. D. A. Molodov, B. B. Straumal, and L. S. Shvindlerman, Scr. Met. **18**, 207 (1984).
47. M. Kamrani, V. I. Levitas, and B. Feng, Mater. Sci. Eng. A **705**, 219 (2017).
48. V. I. Levitas and A. M. Roy, Phys. Rev. B **91**, 174109 (2015).
49. V. I. Levitas, Int. J. Plast. **106**, 164 (2018).

Translated by R. Tyapaev